Soft Matter

PAPER

View Article Online
View Journal

Cite this: DOI: 10.1039/d5sm01195g

Electric-field-induced switching of circularly polarized luminescence in a multicomponent emissive liquid-crystal system

Issei Nakano,[a] Shufang Huang,[b] Daiya Suzuki,[a] Kosuke Kaneko,[c] Junki Maegawa,[b] Soichiro Kawamorita, *[b] Shuichi Suzuki[b] and Yoshitane Imai *[a]

Chiral liquid crystals (LCs) are indispensable functional materials for advanced optoelectronic devices. However, their integration with metal-based emitters remains largely unexplored, limiting the understanding of the influence of external electric fields on different photophysical regimes. In this study, we prepared emissive chiral LC materials by doping two achiral platinum(II) complexes—*trans*-bis(*N*-isopropyl-5-iminomethyl-1*H*-pyrazolato)platinum(II) and *cis*-bis(*N*-methyl-5-iminomethyl-1*H*-pyrazolato)platinum(II)—into a chiral nematic LC host (N* LC) composed of achiral 4′-pentyl-4-biphenylcarbonitrile and chiral 2-octyl-4-[4-(hexyloxy)benzoyloxy]benzoate (2OHBB). Although both platinum complexes are intrinsically achiral luminophores, the resulting N* LC materials exhibited pronounced circularly polarized luminescence (CPL). Remarkably, these CPL-active chiral LC systems demonstrated continuous and fully reversible modulation of their CPL characteristics upon application or removal of a direct-current (DC) electric field. In addition to the chiral induction originating from 2OHBB, the handedness of CPL emission could be reversibly switched by toggling the DC field (ON–OFF–ON). This behaviour is attributable to a reversible phase transition between distinct ordered helical structures within the chiral nematic phase. By combining organic platinum emitters and N* LC matrices, this work broadens the design space for CPL control and advances the materials science underpinning electrically switchable CPL devices

Received 3rd December 2025,
Accepted 5th February 2026

DOI: 10.1039/d5sm01195g

rsc.li/soft-matter-journal

Introduction

Liquid crystals (LCs) are highly versatile soft materials that play a central role in the development of advanced optoelectronic devices.[1–13] When chirality is introduced into a nematic liquid crystal (N-LC)—either by using intrinsically chiral mesogens or by doping with an appropriate chiral additive—the system spontaneously forms a helical superstructure, yielding a chiral nematic LC (N* LC). Within such helical architectures, achiral luminophores adopt helically biased alignments, enabling the emergence of circularly polarized luminescence (CPL) from otherwise achiral emitters.[14–19] The handedness of the helical structure in an N* LC is dictated by the chirality of the constituent LC molecules or chiral dopant. Consequently, the chirality of these molecular components determines whether the embedded luminophores adopt a right-handed or left-handed helical arrangement, which, in turn, fixes the handedness (right- or left-circular) of the resulting CPL emission.

Recent studies have focused on the development of N* LC–based CPL materials whose chiroptical properties can be modulated through external stimuli such as direct-current (DC) electric fields, as well as thermal or optical inputs. This interest is attributable to the dynamic photoluminescence (PL) and CPL responses exhibited by these systems. Because they can reversibly switch CPL characteristics in response to external perturbations, N* LC–CPL materials are regarded as promising candidates for stimulus-responsive chiroptical switching.[20–39]

Previously, we demonstrated ON–OFF switching and handedness inversion of CPL in an N* LC–CPL material obtained by doping a chiral perylene diimide luminophore into the achiral liquid crystal 4′-pentyl-4-biphenylcarbonitrile (5CB).[40] We later developed N* LC–CPL systems by introducing the chiral dopant 2-octyl-4-[4-(hexyloxy)benzoyloxy]benzoate (2OHBB) into 5CB and subsequently incorporating various achiral aromatic luminophores.[41] The CPL characteristics of these N* LC–CPL materials could also be controlled *via* external stimuli.

The present study was aimed at expanding the versatility of the 5CB/2OHBB-based N* LC platform and realizing more

[a] *Department of Applied Chemistry, Faculty of Science and Engineering, Kindai University, 3-4-1 Kowakae, Higashi-Osaka, Osaka 577-8502, Japan. E-mail: y-imai@apch.kindai.ac.jp*
[b] *Department of Chemistry, Graduate School of Engineering Science, The University of Osaka, Machikaneyama, Toyonaka, Osaka 560-8531, Japan. E-mail: kawamorita@chem.es.osaka-u.ac.jp*
[c] *College of Liberal Arts and Sciences, Kitasato University, 1-15-1 Kitasato, Sagamihara, Kanagawa, 228-8555, Japan*

sensitive CPL switching behaviour. To this end, we replaced conventional aromatic organic luminophores with achiral organoplatinum emitters as dopants for the LC host. The selected achiral platinum(II) complexes—*trans*-bis(*N*-isopropyl-5-iminomethyl-1*H*-pyrazolato)platinum(II) (*trans*-[Pt(IPz-iPr)$_2$]) and *cis*-bis(*N*-methyl-5-iminomethyl-1*H*-pyrazolato)platinum(II) (*cis*-[Pt(IPz-Me)$_2$])—are planar Pt(II) complexes featuring π-conjugated systems. These complexes exhibit strong spin–orbit coupling and distinct excited-state characteristics arising from the metal centre, rendering them suitable for enhancing and modulating the CPL behaviour of N* LC–based systems.

Compared with conventional organic π-conjugated luminophores, metal complexes, particularly Pt(II) systems, exhibit inherently different excited-state dynamics, arising from strong spin–orbit coupling, metal–ligand charge-transfer character, and accessible triplet states. These metal-complex-specific photophysical features can drastically alter how the emitter interacts with the chiral nematic field. Thus, introducing Pt(II) complexes into an N* LC host is not simply a substitution of luminophores. This strategy can facilitate the exploration of distinct regimes of chiroptical behaviour. Incorporating such complexes is expected to yield insights, otherwise unattainable with purely organic molecules, into their alignment within the helical superstructure and their influence on CPL switching responses.

Considering these aspects, we fabricated emissive N* LC systems (N*-LC-5CB/2OHBB/*trans*-[Pt(IPz-iPr)$_2$] and N*-LC-5CB/2OHBB/*cis*-[Pt(IPz-Me)$_2$]) by doping the achiral luminophores *trans*-[Pt(IPz-iPr)$_2$] and *cis*-[Pt(IPz-Me)$_2$] into a mixed N* LC host composed of the achiral LC 5CB and chiral LC 2OHBB (Fig. 1). Because 2OHBB is a solid at room temperature, the LC phase was obtained by blending it with 5CB. The optical and electric-field-responsive properties of the resulting materials were systematically investigated. Both emissive chiral LC systems exhibited continuous and fully reversible switching of CPL handedness in response to an applied DC electric field.

Results and discussion

By doping *trans*-[Pt(IPz-iPr)$_2$] and *cis*-[Pt(IPz-Me)$_2$] into N* LC hosts composed of 5CB/(*R*)-2OHBB = 98/2 mol% or 5CB/(*S*)-2OHBB = 98/2 mol% at a concentration of 1.0×10^{-2} M relative to 5CB, we successfully prepared four types of N* LC materials: N*-LC-5CB/(*R*)-2OHBB/*trans*-[Pt(IPz-iPr)$_2$], N*-LC-5CB/(*S*)-2OHBB/*trans*-[Pt(IPz-iPr)$_2$], N*-LC-5CB/(*R*)-2OHBB/*cis*-[Pt(IPz-Me)$_2$], and N*-LC-5CB/(*S*)-2OHBB/*cis*-[Pt(IPz-Me)$_2$] (4.2 and 3.7 wt% for *trans*-[Pt(IPz-iPr)$_2$] and *cis*-[Pt(IPz-Me)$_2$], respectively). These N* LC samples were then introduced into conductive indium tin oxide (ITO) glass cells to fabricate the corresponding N* LC devices.

To evaluate the LC properties of the obtained N* LC materials, polarized optical microscopy (POM) images of N*-LC-5CB/(*R*)-2OHBB/*trans*-[Pt(IPz-iPr)$_2$] and N*-LC-5CB/(*R*)-2OHBB/*cis*-[Pt(IPz-Me)$_2$] were recorded at 25 °C (Fig. 2(a) and (b)). In both N* LC devices, characteristic fingerprint textures indicative of the N* phase were clearly observed. These results confirm that the achiral 5CB matrix forms a helical superstructure through efficient chiral induction from (*R*)-2OHBB.

The systems doped with *trans*-[Pt(IPz-iPr)$_2$] and *cis*-[Pt(IPz-Me)$_2$] showed similar fingerprint patterns, indicating that neither the substituent environment nor the geometric isomerism of these platinum emitters considerably perturbs the helical organization of the N* LC host. This observation suggests that, although these complexes differ in both geometry and substituents, the differences do not significantly affect the LC alignment or resulting CPL characteristics.

To investigate the helical orientation of the chiral nematic phase, contact tests were conducted using cholesteryl oleyl carbonate (left-handed helical sense) as a standard material (Fig. S1). The LC mixture filled in the left part of the glass cell was placed in contact with the standard material from the right side. When (*S*)-2OHBB was used with N*-LC-5CB/(*S*)-2OHBB, a continuous LC texture was observed, owing to the identical helical orientation (Fig. SI-1(a) and SI-1(c)). In contrast, using (*R*)-2OHBB with N*-LC-5CB/(*R*)-2OHBB resulted in a discontinuous LC texture (Fig. SI-1(b) and SI-1(d)). These results suggest that N*-LC-5CB/(*S*)-2OHBB forms a left-handed helical sense and N*-LC-5CB/(*R*)-2OHBB forms a right-handed helical sense in the N* phase.

Next, we investigated the chiroptical properties of N*-LC-5CB/2OHBB/*trans*-[Pt(IPz-iPr)$_2$] and N*-LC-5CB/2OHBB/*cis*-[Pt(IPz-Me)$_2$] (Fig. 3(a) and 4(a)). Both systems exhibited intense PL. As anticipated, despite the use of intrinsically achiral luminophores, strong CPL was observed from both N* LC devices. The CPL responses of N*-LC-5CB/2OHBB/*trans*-[Pt(IPz-iPr)$_2$] and N*-LC-5CB/2OHBB/*cis*-[Pt(IPz-Me)$_2$] were characterized by electronic transition bands intrinsic to each

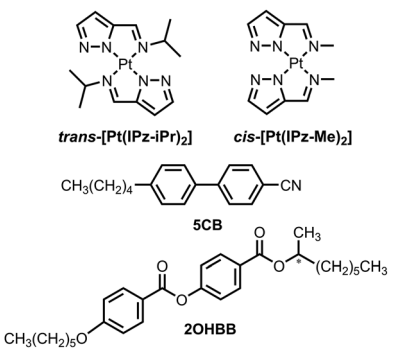

Fig. 1 Chemical structures of the achiral luminophores *trans*-[Pt(IPz-iPr)$_2$] and *cis*-[Pt(IPz-Me)$_2$], achiral nematic liquid crystal 5CB, and chiral nematic liquid crystal 2OHBB.

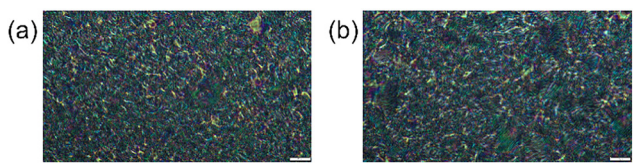

Fig. 2 Polarized optical microscopy (POM) images of (a) N*-LC-5CB/(*R*)-2OHBB/*trans*-[Pt(IPz-iPr)$_2$] and (b) N*-LC-5CB/(*R*)-2OHBB/*cis*-[Pt(IPz-Me)$_2$] (50×).

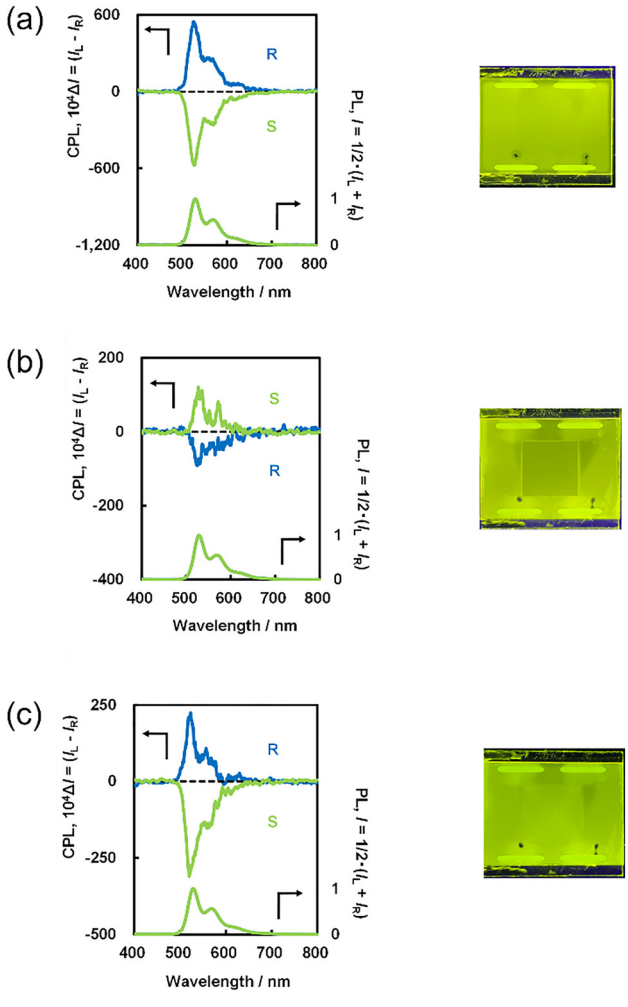

Fig. 3 Circularly polarized luminescence (CPL, top) and photoluminescence (PL, bottom) spectra of N*-LC-5CB/(*R*)-2OHBB/*trans*-[Pt(IPz-iPr)$_2$] (blue) and N*-LC-5CB/(*S*)-2OHBB/*trans*-[Pt(IPz-iPr)$_2$] (green), together with corresponding emission photographs. (a) Before voltage application (0 V), (b) under an applied voltage of 30 V, and (c) after removal of the voltage (0 V). The excitation wavelength for the CPL spectra, PL spectra, and emission photographs was 365 nm.

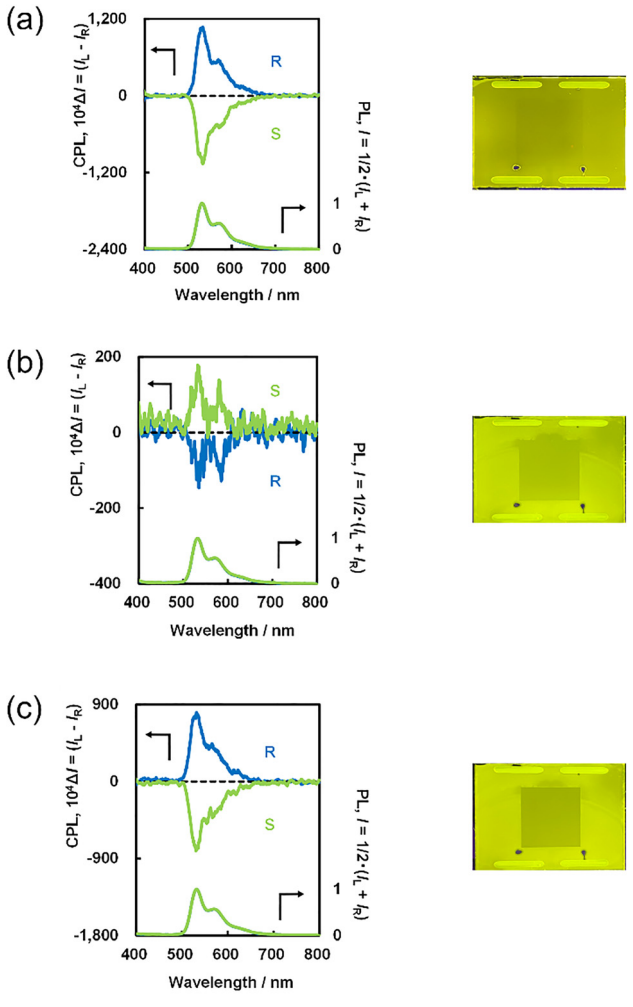

Fig. 4 Circularly polarized luminescence (CPL, top) and photoluminescence (PL, bottom) spectra of N*-LC-5CB/(*R*)-2OHBB/*cis*-[Pt(IPz-Me)$_2$] (blue) and N*-LC-5CB/(*S*)-2OHBB/*cis*-[Pt(IPz-Me)$_2$] (green), together with corresponding emission photographs. (a) Before voltage application (0 V), (b) under an applied voltage of 30 V, and (c) after removal of the voltage (0 V). The excitation wavelengths were 360 nm for CPL and PL measurements and 365 nm for the emission photographs.

complex. The CPL spectra of the (*R*)-2OHBB- and (*S*)-2OHBB-based N* LC systems were essentially mirror images of one another. The CPL maxima (λ_{CPL}) were approximately 526 nm and 534 nm for the *trans*-[Pt(IPz-iPr)$_2$] and *cis*-[Pt(IPz-Me)$_2$] systems, respectively.

Both N* LC materials doped with *trans*-[Pt(IPz-iPr)$_2$] or *cis*-[Pt(IPz-Me)$_2$] displayed CPL signals of the same sign originating from their chiral T_1 excited states: N*-LC-5CB/(*R*)-2OHBB/*trans*-[Pt(IPz-iPr)$_2$] and N*-LC-5CB/(*R*)-2OHBB/*cis*-[Pt(IPz-Me)$_2$] showed positive (+) CPL, whereas the corresponding (*S*)-systems exhibited negative (−) CPL. Notably, for all N*-LC-5CB/2OHBB devices, the CPL spectra measured from both sides of the ITO cell were identical, indicating that artifacts such as linear birefringence were negligible under the present measurement conditions.[41]

The intensity of circular polarization in the excited state is typically quantified by the anisotropic dissymmetry factor (*g*-factor), defined as $g_{CPL} = \Delta I/I = 2(I_L - I_R)/(I_L + I_R)$, where I_L and I_R denote the emission intensities of left- and right-circularly polarized components, respectively, under unpolarized excitation.

The $|g_{CPL}|$ values for N*-LC-5CB/2OHBB/*trans*-[Pt(IPz-iPr)$_2$] and N*-LC-5CB/2OHBB/*cis*-[Pt(IPz-Me)$_2$] were approximately 0.06 at 526 nm and 0.12 at 534 nm, respectively. These comparable $|g_{CPL}|$ values correlate well with the similar fingerprint textures observed for the two systems, including their nearly identical stripe widths (Fig. 2). The $|g_{CPL}|$ values for the present N* LC devices, which are of the order of 10^{-1}, are consistent with those previously reported for N*-LC-5CB/2OHBB systems.[41]

Within the N* LC medium, the LC environment likely stabilizes the emitter molecules and suppresses nonradiative

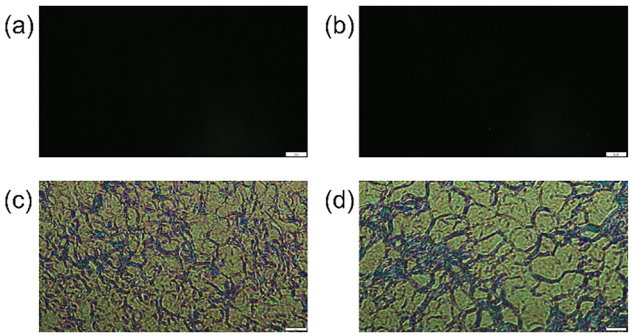

Fig. 5 Polarized optical microscopy (POM) images obtained (a) and (b) under an applied direct-current voltage of 30 V and (c) and (d) after removal of the voltage (0 V). (a) N*-LC-5CB/(*R*)-2OHBB/*trans*-[Pt(IPz-iPr)$_2$], (b) N*-LC-5CB/(*R*)-2OHBB/*cis*-[Pt(IPz-Me)$_2$], (c) N*-LC-5CB/(*R*)-2OHBB/*trans*-[Pt(IPz-iPr)$_2$], and (d) N*-LC-5CB/(*R*)-2OHBB/*cis*-[Pt(IPz-Me)$_2$]. Magnification: 50×.

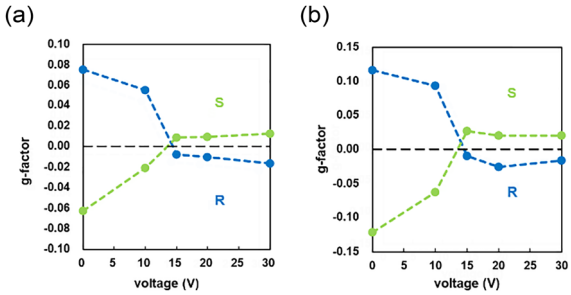

Fig. 6 g_{CPL} values for applied voltage ranging from 0 V to 30 V. (a) N*-LC-5CB/(*R*)-2OHBB/*trans*-[Pt(IPz-iPr)$_2$] (blue) and N*-LC-5CB/(*S*)-2OHBB/*trans*-[Pt(IPz-iPr)$_2$] (green) and (b) N*-LC-5CB/(*R*)-2OHBB/*cis*-[Pt(IPz-Me)$_2$] (blue) and N*-LC-5CB/(*S*)-2OHBB/*cis*-[Pt(IPz-Me)$_2$] (green). The monitored wavelengths were 529 nm and 531 nm for the *trans*-[Pt(IPz-iPr)$_2$] and *cis*-[Pt(IPz-Me)$_2$] systems, respectively. Excitation wavelengths were 365 nm and 360 nm for the *trans*-[Pt(IPz-iPr)$_2$] and *cis*-[Pt(IPz-Me)$_2$] systems, respectively.

decay pathways, and the helical superstructure induces a chiral spatial arrangement of the achiral luminophores. These combined effects likely contribute to the large $|g_{CPL}|$ values obtained.

Next, we examined the modulation of CPL characteristics under an applied DC electric field using N*-LC-5CB/2OHBB/*trans*-[Pt(IPz-iPr)$_2$] and N*-LC-5CB/2OHBB/*cis*-[Pt(IPz-Me)$_2$]. When a DC voltage of 30 V was applied to these N* LC devices, the POM images displayed significant changes, indicating structural transitions within the helical superstructure in the N* LC systems (Fig. 5(a) and (b)). Because the LC host consists predominantly of 5CB (98 mol%), the response of the LC host to an applied DC electric field is expected to be governed mainly by 5CB, which exhibits positive dielectric anisotropy. The dark POM textures observed under the applied electric field are thus consistent with a field-induced homeotropic alignment of the LC host.

At an applied voltage of 30 V, both devices exhibited a decrease in the CPL intensity and magnitude of $|g_{CPL}|$ (Fig. 3(b) and (b)). In contrast, the CPL spectra of the (*R*)- and (*S*)-systems largely retained their mirror-image relationship. Interestingly, application of the 30 V external field resulted in a complete inversion of the CPL sign. Specifically, the g_{CPL} value for N*-LC-5CB/2OHBB/*trans*-[Pt(IPz-iPr)$_2$] was −0.011 at 527 nm, whereas that for N*-LC-5CB/2OHBB/*cis*-[Pt(IPz-Me)$_2$] was −0.016 at 535 nm.

Notably, for both luminophores, when measurements were carried out under applied voltages of 0, 10, 15, 20, and 30 V, a reversal of the CPL spectral sign was observed between 10 and 15 V, and the extent of the decrease was not linear (Fig. 6).

Upon removing the applied voltage (returning to 0 V), both the CPL intensity and $|g_{CPL}|$ values recovered toward their initial states, reaching approximately 0.034 at 522 nm for N*-LC-5CB/2OHBB/*trans*-[Pt(IPz-iPr)$_2$] and 0.08 at 532 nm for N*-LC-5CB/2OHBB/*cis*-[Pt(IPz-Me)$_2$] (Fig. 3(c) and 4(c)). The corresponding POM images after voltage removal resembled those recorded before voltage application (Fig. 5(c) and (d)).

CPL measurements were conducted under repeated OFF–ON voltage cycling to evaluate the reversibility and continuity of the CPL switching behaviour. As shown in Fig. 7, both devices exhibited fully reversible and continuous CPL switching, with response times within 1 s. These findings demonstrate that, in the N*-LC-5CB/2OHBB systems, both the magnitude and handedness of CPL emission can be continuously and reversibly controlled through the application of a DC electric field.

The CPL switching behaviour observed in these systems can be rationalized as follows. In the N*-LC-5CB/2OHBB matrix, the achiral emitters *trans*-[Pt(IPz-iPr)$_2$] and *cis*-[Pt(IPz-Me)$_2$] are chirally oriented along the helical superstructure formed by the rod-like 5CB and 2OHBB mesogens. The conjugated planes of the emitters adopt a unidirectionally twisted alignment while

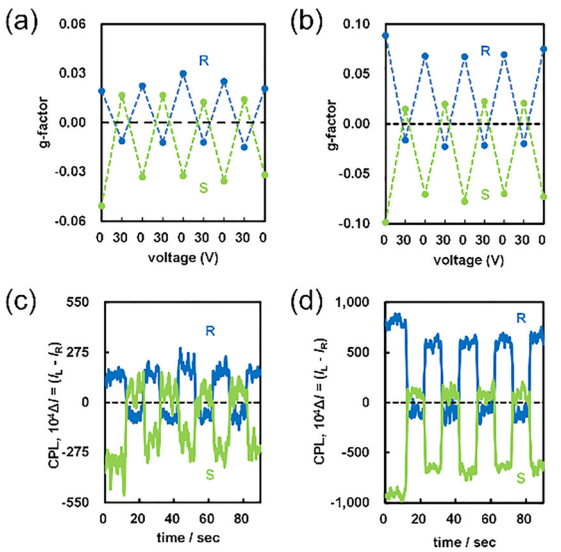

Fig. 7 CPL intensity switching (a) and (b) and g_{CPL} switching (c) and (d) under repeated voltage cycling between 0 V and 30 V at 10 s intervals. (a) and (c) N*-LC-5CB/(*R*)-2OHBB/*trans*-[Pt(IPz-iPr)$_2$] (blue) and N*-LC-5CB/(*S*)-2OHBB/*trans*-[Pt(IPz-iPr)$_2$] (green). (b) and (d) N*-LC-5CB/(*R*)-2OHBB/*cis*-[Pt(IPz-Me)$_2$] (blue) and N*-LC-5CB/(*S*)-2OHBB/*cis*-[Pt(IPz-Me)$_2$] (green). The monitored wavelengths were 529 nm and 531 nm for the *trans*-[Pt(IPz-iPr)$_2$] and *cis*-[Pt(IPz-Me)$_2$] systems, respectively. Excitation wavelengths were 365 nm and 360 nm for the *trans*-[Pt(IPz-iPr)$_2$] and *cis*-[Pt(IPz-Me)$_2$] systems, respectively.

remaining nearly parallel, resulting in a chiral relative arrangement that follows the helical axis of the N* LC. This chiral organization of the luminophores likely results in the strong CPL signals observed.

Although the *trans*- and *cis*-Pt complexes differ in both coordination geometry and substituents, these differences do not significantly perturb the N* LC alignment. The observed differences in $|g_{CPL}|$ values are instead attributable to variations in excited-state coupling between the Pt complexes and chiral LC host, influenced by differences in triplet-state lifetimes and steric effects of the substituents.

Upon application of a DC electric field, the LC host reorients to a homeotropic configuration, causing both 5CB and 2OHBB to align perpendicular to the ITO substrates. This field-induced reorientation disrupts the helical superstructure and places the Pt complexes nearly perpendicular to the substrate, changing the projection of their transition dipole moments onto the observation axis. Consequently, g_{CPL} inverts and the CPL intensity decreases as the emitters experience a weakly chiral local environment. In this context, the Pt complexes primarily function as emissive probes of the chiral nematic field, where their triplet-state emission enables efficient transduction of the LC-induced chiral environment into CPL signals. These orientation transitions are supported by the corresponding POM images.

Conclusion

We developed N* LC emissive materials exhibiting strong CPL by doping achiral Pt-based π-extended luminophores *trans*-[Pt(IPz-iPr)$_2$] and *cis*-[Pt(IPz-Me)$_2$] into an N* LC host composed of achiral 5CB and chiral 2OHBB. The resulting N*-LC-5CB/2OHBB/*trans*-[Pt(IPz-iPr)$_2$] and N*-LC-5CB/2OHBB/*cis*-[Pt(IPz-Me)$_2$] systems exhibited high anisotropic dissymmetry factors ($g_{CPL} \approx 0.06$ and 0.12, respectively), demonstrating that the metal–organic dopants strongly interact with the helical order of the N* phase and undergo efficient chiral induction. Application of a DC electric field enabled continuous and fully reversible CPL switching through ON–OFF–ON voltage cycling. This switching behaviour originates from the field-induced transformation of the helical superstructure in the N* LC, indicating that N* LC systems doped with metal-complex luminophores can serve as responsive and reversible CPL-switchable media.

Overall, our findings reveal that N* LC materials incorporating metal-containing π-extended emitters can simultaneously achieve strong CPL emission and electric-field-responsive switching. The insights gained from this work provide valuable guidelines for advanced CPL control, design of switchable CPL devices, and development of next-generation chiroptical photonic materials.

Experimental

General

Melting points were measured on a glass plate using a Yanagimoto micro–melting point apparatus. Infrared (IR) spectroscopy was performed using a Jasco FT/IR-410 spectrometer. ^{1}H and ^{13}C nuclear magnetic resonance (NMR) spectra were recorded on a Varian Unity–Inova 500 spectrometer (500 MHz for ^{1}H, 125 MHz for ^{13}C), as well as a JEOL ECZ-500 (500 MHz for ^{1}H, 125 MHz for ^{13}C). Chemical shifts are reported in δ-unit (ppm) relative to tetramethylsilane (Fig. S2 and S3). The splitting patterns are designated as follows: s (singlet), d (doublet), t (triplet), q (quartet), m (multiplet), and br (broad).

Materials

$PtCl_2(CH_3CN)_2$ was prepared according to a previously reported procedure.[42] 1*H*-pyrazole-3-carboxaldehyde (Apollo Scientific), 40% methylamine aqueous solution (Fujifilm Wako Pure Chemical), isopropylamine (Tokyo Chemical Industry), ethanol, potassium carbonate, dimethyl sulfoxide (DMSO), toluene, *n*-hexane, and ethyl acetate were purchased from commercial suppliers and used without further purification. 5CB, (*R*)-2OHBB, and (*S*)-2OHBB (Tokyo Chemical Industry) were also purchased from commercial suppliers and used without further purification. ITO cells for electric-field experiments (model: KSSZ-10/B107P1NSS05) were purchased from EHC Co., Ltd. (Tokyo, Japan).

X-ray structure determination

The stereochemical arrangements of *trans*-[Pt(IPz-iPr)$_2$] and *cis*-[Pt(IPz-Me)$_2$] were established by X-ray structure determination. Crystals used for the analysis were obtained by recrystallization from an ethyl acetate/chloroform solution for *trans*-[Pt(IPz-iPr)$_2$] and dimethylsulfoxide for *cis*-[Pt(IPz-Me)$_2$]. Data were collected using an XtaLAB P-200 diffractometer (Rigaku Corporation, Tokyo, Japan) with graphite-monochromated Mo Kα radiation (λ = 0.71075 Å). The structures were solved using direct methods and refined using the full-matrix least-squares method. In the subsequent refinement, the function $\sum\omega(F_o^2-F_c^2)^2$ was minimized, where F_o and F_c represent the observed and calculated structure-factor amplitudes, respectively. The positions of non-hydrogen atoms were determined from difference-Fourier electron-density maps and refined anisotropically. ORTEP drawings of the molecular structures are provided in Fig. S4, and detailed crystallographic parameters are summarized in Table S1. Crystallographic data for *trans*-[Pt(IPz-*i*Pr)$_2$] (CCDC 2505189) and *cis*-[Pt(IPz-Me)$_2$] (CCDC 2505190) are available free of charge from the Cambridge Crystallographic Data Centre. ORTEP illustrations were generated using ORTEP-3.

Synthesis of *trans*-[Pt(IPz-iPr)$_2$]

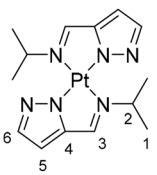

A solution of 1*H*-pyrazole-3-carboxaldehyde (325 mg, 3.38 mmol) and isopropylamine (198 mg, 3.35 mmol) in ethanol (35.0 mL) was refluxed at 100 °C for 2 h. After cooling in an ice bath, the solvent was removed under reduced pressure to yield a crude product (432 mg, 3.15 mmol). The residue was dissolved in DMSO (50 mL) and toluene (200 mL) and then

treated with $PtCl_2(CH_3CN)_2$ (550 mg, 1.58 mmol) and K_2CO_3 (1.39 g, 10.1 mmol). The mixture was refluxed at 140 °C for 20 h and then cooled in an ice bath. Water and ethyl acetate were added, and the organic layer was separated and washed with brine. The combined organic extracts were dried and concentrated under reduced pressure. The crude product was purified by recrystallization from EtOAc/$CHCl_3$ to afford *trans*-[Pt(IPz-iPr)$_2$] as yellow crystals (244 mg, 0.522 mmol, 33%). The *cis* isomer was not observed under these conditions.

M.p. 265 °C (Decomp.). IR (KBr): 775, 930, 988, 1044, 1114, 1134, 1152, 1173, 1267, 1359, 1379, 1061, 2871, 2967, 3006 cm^{-1}. ^1H NMR ($CDCl_3$, 500 MHz): δ 1.50 (d, J = 6.6 Hz, 12 H, H^1), 5.72 (sptd, J = 6.6, 1.0 Hz, 2 H, H^2), 6.65 (d, J = 2.0 Hz, 2 H, H^5), 7.68 (d, J = 2.0 Hz, 2 H, H^6), 8.00 (d, J = 1.0 Hz, 2 H, H^3). ^{13}C NMR ($CDCl_3$, 125 MHz): δ 23.2 (C^1), 55.6 (C^2), 108.0 (C^5), 138.8 (C^6), 149.8 (C^4), 157.4 (C^3).

HRMS (APCI): m/z Calcd for $C_{14}H_20N_6{}^{195}Pt$: 468.1471. Found: 468.1458 $[M]^+$. Anal. Calcd for $C_{14}H_20N_6Pt$: C, 35.97; H, 4.31; N, 17.98. Found: C, 35.89; H, 4.18; N, 17.87.

Synthesis of *cis*-[Pt(IPz-Me)$_2$]

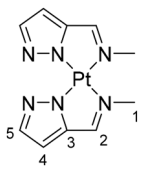

A solution of 1*H*-pyrazole-3-carboxaldehyde (490 mg, 5.10 mmol) and 40% aqueous methylamine (375 mg, 4.83 mmol) in ethanol (50 mL) was refluxed at 100 °C for 2 h. After cooling in an ice bath, the solvent was removed under reduced pressure to yield a crude product (531 mg, 4.86 mmol). The residue was dissolved in DMSO (75 mL) and toluene (300 mL) and treated with $PtCl_2(CH_3CN)_2$ (870 mg, 2.50 mmol) and K_2CO_3 (2.15 g, 15.6 mmol). The mixture was refluxed at 140 °C for 24 h and then cooled in an ice bath. Water and ethyl acetate were added, and the organic layer was separated and washed with brine. The combined organic extracts were dried and concentrated under reduced pressure. The crude product was purified by recrystallization from DMSO to afford *cis*-[Pt(IPz-Me)$_2$] as red crystals (64.9 mg, 0.158 mmol, 6%). The *trans*-isomer was not observed under these conditions.

M.p. 261 °C (Decomp.). IR (KBr): 698, 737, 805, 905, 930, 1033, 1046, 1143, 1214, 1268, 1340, 1362, 1415, 1622, 2929 cm^{-1}. ^1H NMR (DMSO-d_6, 500 MHz): δ 3.99 (d, J = 1.2 Hz, 6 H, H^1), 6.68 (d, J = 2.0 Hz, 2 H, H^4), 7.59 (d, J = 2.0 Hz, 2 H, H^5), 8.40 (q, J = 1.2 Hz, 2 H, H^2). ^{13}C NMR (DMSO-d_6, 125 MHz): δ 47.9 (C^1), 108.3 (C^4), 138.5 (C^5), 148.9 (C^6), 164.5 (C^2).

HRMS (APCI): m/z Calcd for $C_{10}H_{12}N_6{}^{195}Pt$: 412.0844. Found: 412.0860 $[M]^+$. Anal. Calcd for $C_{10}H_{12}N_6Pt$: C, 29.20; H, 2.94, N, 20.43. Found: C, 29.18, H, 2.53, N, 20.17.

Preparation of N*-LC-5CB/2OHBB/*trans*-[Pt(IPz-iPr)$_2$] and N*-LC-5CB/2OHBB/*cis*-[Pt(IPz-Me)$_2$]

A mixed LC host was prepared by adding *trans*-[Pt(IPz-iPr)$_2$] (or *cis*-[Pt(IPz-Me)$_2$]) to a 5CB:(*R*)-2OHBB mixture (98 : 2 molar ratio) at a concentration of 1.0×10^{-2} M relative to 5CB, followed by dissolution at 40 °C. The same procedure was used to prepare the mixtures containing (*S*)-2OHBB. The resulting LC mixtures were introduced into ITO cells (KSSZ-10/B107P1NSS05) by applying 1–2 drops of the mixture to fabricate the LC devices.

PL and CPL spectroscopy of N*-LC-5CB/2OHBB/*trans*-[Pt(IPz-iPr)$_2$] and N*-LC-5CB/2OHBB/*cis*-[Pt(IPz-Me)$_2$]

PL and CPL spectra of the LC samples were recorded at 25 °C using a JASCO CPL-300 spectrofluoropolarimeter (Tokyo, Japan) at a scattering angle of 0°. Samples were excited with unpolarized monochromatic light. For LC measurements, the excitation and emission bandwidths were set to 0.5 nm and 10 nm, respectively. The scan speed was 100 nm min^{-1}, and the photomultiplier tube time constant under applied voltage conditions was set as 4 s. The excitation wavelengths were 365 nm for the N*-LC-5CB/2OHBB/*trans*-[Pt(IPz-iPr)$_2$] devices and 360 nm for the N*-LC-5CB/2OHBB/*cis*-[Pt(IPz-Me)$_2$] devices. A DC voltage was applied using an ADCMT 6241A DC voltage/current source and monitor.

Characterization of LC textures

The optical textures of the LC phases were observed using an Olympus BX53 polarized optical microscope (Japan) equipped with a hot stage. The LC materials were filled into ITO cells, which were used to acquire POM images under applied voltage. The electrode gap of the ITO cells was 10 μm.

Conflicts of interest

There are no conflicts to declare.

Data availability

The data supporting this article have been uploaded as part of the supplementary information (SI). Supplementary information is available. DOI: https://doi.org/10.1039/d5sm01195g.

CCDC 2505189 and 2505190 contain the supplementary crystallographic data for this paper.[43a,b]

Acknowledgements

This work was supported by a JST-CREST grant (Grant Number JPMJCR2001), a Grant-in-Aid for Scientific Research (KAKENHI; Grant Numbers JP23H02040 and JP24K08087) from MEXT and JSPS, an IZUMI SCIENCE and TECHNOLOGY Foundation Research Grant (Grant Number 2024-J-062), and the Fujikura Foundation Research Grant (Grant Number 202514).

Notes and references

1 L. M. Blinov and V. G. Chigrinov, *Electrooptic Effects in Liquid Crystal Materials*, Springer, New York, 1996.
2 C. Weder, C. Sarwa, A. Montali, C. Bastiaansen and P. Smith, *Science*, 1998, **279**, 835–837.

3 M. Grell and D. D. C. Bradley, *Adv. Mater.*, 1999, **11**, 895–905.
4 P. Fischer and F. Hache, *Chirality*, 2005, **17**, 421–437.
5 S. Relaix, C. Bourgerette and M. Mitov, *Appl. Phys. Lett.*, 2006, **89**, 251907.
6 M. Goh, T. Matsushita, M. Kyotani and K. Akagi, *Macromolecules*, 2007, **40**, 4762–4771.
7 K. Akagi, *Chem. Rev.*, 2009, **109**, 5354–5401.
8 C. Mowatt, S. M. Morris, M. H. Song, T. D. Wilkinson, R. H. Friend and H. J. Coles, *J. Appl. Phys.*, 2010, **107**, 043101.
9 T. Geelhaar, K. Griesar and B. Reckmann, *Angew. Chem., Int. Ed.*, 2013, **52**, 8798–8809.
10 Y. Chen, J. Lin, W. Yuan, Z. Yu, J. W. Lam and B. Z. Tang, *Sci. China: Chem.*, 2013, **56**, 1191–1196.
11 J. W. Goodby, P. J. Collings, T. Kato, C. Tschierske, H. Gleeson and P. Raynes, *Handbook of Liquid Crystals*, Wiley-VCH Press, Weinheim, 2nd edn, 2014.
12 Z. Wang, T. Xu, A. Noel, Y.-C. Chen and T. Liu, *Soft Matter*, 2021, **17**, 4675–4702.
13 T. Bezrodna, V. Melnyk, V. Vorobjev and G. Puchkovska, *J. Lumin.*, 2010, **130**, 1134–1141.
14 D. Zhao, F. Fan, J. Cheng, Y. Zhang, K. S. Wong, V. G. Chigrinov, H. S. Kwok, L. Guo and B. Z. Tang, *Adv. Opt. Mater.*, 2015, **3**, 199–202.
15 D. Y. Zhao, H. G. He, X. G. Gu, L. Guo, K. S. Wong, J. W. Y. Lam and B. Z. Tang, *Adv. Opt. Mater.*, 2016, **4**, 534–539.
16 Y. H. Shi, P. F. Duan, S. W. Huo, Y. G. Li and M. H. Liu, *Adv. Mater.*, 2018, **30**, e1705011.
17 X. J. Li, Q. Li, Y. X. Wang, Y. W. Quan, D. Z. Chen and Y. X. Cheng, *Chemistry*, 2018, **24**, 12607–12612.
18 Q. X. Jin, S. X. Chen, Y. T. Sang, H. Q. Guo, S. Z. Dong, J. L. Han, W. J. Chen, X. F. Yang, F. Li and P. F. Duan, *Chem. Commun.*, 2019, **55**, 6583–6586.
19 Y. Wu, M. Li, Z.-G. Zheng, Z.-Q. Yu and W.-H. Zhu, *J. Am. Chem. Soc.*, 2023, **145**, 12951–12966.
20 Y. Zhou, Y. Wang, Y. Song, S. Zhao, M. Zhang, G. Li, Q. Guo, Z. Tong, Z. Li, S. Jin, H.-B. Yao, M. Zhu and T. Zhuang, *Nat. Commun.*, 2024, **15**, 251.
21 N. Y. Ha, Y. Ohtsuka, S. M. Jeong, S. Nishimura, G. Suzaki, Y. Takanishi, K. Ishikawa and H. Takezoe, *Nat. Mater.*, 2007, **7**, 43–47.
22 R. K. Vijayaraghavan, S. Abraham, H. Akiyama, S. Furumi, N. Tamaoki and S. Das, *Adv. Funct. Mater.*, 2008, **18**, 2510–2517.
23 A. Bobrovsky, K. Mochalov, V. Oleinikov, A. Sukhanova, A. Prudnikau, M. Artemyev, V. Shibaev and I. Nabiev, *Adv. Mater.*, 2012, **24**, 6216–6222.
24 J. Yan, F. Ota, B. A. S. San Jose and K. Akagi, *Adv. Funct. Mater.*, 2017, **27**, 1604529.
25 J. Li, H. K. Bisoyi, J. Tian, J. Guo and Q. Li, *Adv. Mater.*, 2019, **31**, e1807751.
26 T. Hamamoto and M. Funahashi, *J. Mater. Chem. C*, 2015, **3**, 6891–6900.
27 H. K. Bisoyi and Q. Li, *Chem. Rev.*, 2016, **116**, 15089–15166.
28 X. Li, Y. Shen, K. Liu, Y. Quan and Y. Cheng, *Mater. Chem. Front.*, 2020, **4**, 2954–2961.
29 L. Wang, A. M. Urbas and Q. Li, *Adv. Mater.*, 2020, **32**, e1801335.
30 X. Yang, M. Zhou, Y. Wang and P. Duan, *Adv. Mater.*, 2020, **32**, e2000820.
31 P. Lu, Y. Chen, Z. Chen, Y. Yuan and H. Zhang, *J. Mater. Chem. C*, 2021, **9**, 6589–6596.
32 K. Yao, Z. Liu, H. Li, D. Xu, W. H. Zheng, Y. W. Quan and Y. X. Cheng, *Sci. China: Chem.*, 2022, **65**, 1945–1952.
33 X. Zhang, Y. Xu, C. Valenzuela, X. Zhang, L. Wang, W. Feng and Q. Li, *Light: Sci. Appl.*, 2022, **11**, 223.
34 J. Liu, Z. P. Song, L. Y. Sun, B. X. Li, Y. Q. Lu and Q. Li, *Responsive Mater.*, 2023, **1**, e20230005.
35 Y. Li, Y. Chen, H. Li, C. Liu, L. Li, Y. Quan and Y. Cheng, *Angew. Chem., Int. Ed.*, 2023, **62**, e202312159.
36 W. Kang, Y. Tang, X. Meng, S. Lin, X. Zhang, J. Guo and Q. Li, A Photo- and Thermo-Driven Azoarene-Based Circularly Polarized Luminescence Molecular Switch in a Liquid Crystal Host, *Angew. Chem., Int. Ed.*, 2023, **62**, e202311486.
37 Y. Chen, P. Lu, Z. Li, Y. Yuan, Q. Ye and H. Zhang, *ACS Appl. Mater. Interfaces*, 2020, **12**, 56604–56614.
38 H. Wang, Z. Chen, Y. Yuan and H. Zhang, *Soft Matter*, 2022, **18**, 5483–5491.
39 B. A. S. Jose, J. Yan and K. Akagi, *Angew. Chem., Int. Ed.*, 2014, **53**, 10641–10644.
40 S. Suzuki, K. Kaneko, T. Hanasaki, M. Shizuma and Y. Imai, *ChemPhotoChem*, 2024, **8**, e202300224.
41 K. Terakubo, H. Nakajima, D. Suzuki, K. Kaneko, T. Hanasaki and Y. Imai, *ChemPhotoChem*, 2025, **9**, e202500112.
42 F. P. Fanizzi, F. P. Intini, L. Maresca and G. Natile, *J. Chem. Soc., Dalton Trans.*, 1990, 199–202.
43 (*a*) CCDC 2505189: Experimental Crystal Structure Determination, 2026, DOI: 10.5517/ccdc.csd.cc2q2vk7; (*b*) CCDC 2505190: Experimental Crystal Structure Determination, 2026, DOI: 10.5517/ccdc.csd.cc2q2vl8.